Density functional study on metastable bcc copper: Electronic structure and momentum density of positron-electron pairs

Z. Tang,[1] M. Hasegawa,[1,2] Y. Nagai,[2] and M. Saito[3]
[1]*Institute for Materials Research, Tohoku University, Sendai 980-8577, Japan*
[2]*The Oarai Branch, Institute for Materials Research, Tohoku University, Oarai, Ibaraki 311-1313, Japan*
[3]*NEC Informatec Systems, Ltd., 34, Miyukigaoka, Tsukuba 305-8501, Japan*
(Received 25 October 2001; published 22 April 2002)

The stability, electronic structure, and positron-electron pair momentum of body-centered-cubic (bcc) copper, which is metastable, are theoretically studied and are compared with those of stable face-centered-cubic (fcc) copper and of ferromagnetic iron (bcc Fe). We first perform electronic structure calculations based on the local-density approximation or generalized gradient approximation (GGA) and find that the GGA well reproduces measured bulk properties, i.e., lattice constants, cohesive energies, and bulk moduli. The calculated cohesive energies of fcc and bcc coppers are very similar and the estimated lattice mismatch between bcc Cu and bcc Fe is very small ($\sim 1.4\%$). These results support previous experimental suggestion that the lattice of bcc Cu precipitates in Fe matrix is nearly coherent to that of the matrix. Next, we calculate momentum-density distributions of positron-electron pairs using the two-component density-functional theory. It is found that the momentum-density distributions of bcc Cu and fcc Cu are very similar but are quite different from that of Fe, which indicates that an analysis of measured coincidence Doppler broadening (CDB) of positron annihilation radiation gives useful information on Cu precipitates in Fe. Actually, by comparing the calculated and measured CDB spectra, we confirm the previous experimental conclusion: In an Fe 1.0 wt % Cu alloy after thermal aging at 550 °C for 2 h, the observed signals originate from the completely confined positrons in bcc Cu precipitates, which annihilate with valence electrons of Cu atoms.

DOI: 10.1103/PhysRevB.65.195108 PACS number(s): 71.20.Be, 78.70.Bj, 81.07.Bc

I. INTRODUCTION

Elemental copper, one of the most important materials for industry, is stable in face-centered-cubic (fcc) structure up to the melting point. The body-centered-cubic (bcc) phase of copper is predicted to be metastable and is of great fundamental interest to both experimental and theoretical solid-state physics, since many aspects of the electronic and structural properties of bcc Cu had been rather controversial. Earlier first-principles calculations of total energy[1,2] found a double-well metastability in bcc Cu, which is, however, not supported by subsequent theoretical studies.[3–6] There were also many experimental attempts[7–10] to realize and to characterize bcc Cu. Recently, this metastable phase has been successfully observed in epitaxial Cu films on Fe (Refs. 7 and 8) and Ag (Ref. 9) substrates and in grain boundaries of fcc Cu bicrystals.[10]

It should be mentioned that such bcc Cu was suggested much earlier as coherent nanosize precipitates in FeCu alloys.[11] The precipitates were found to have a significant effect on the mechanical properties of the host alloys; for instance, they are considered as an origin of the irradiation-induced embrittlements of reactor-pressure-vessel steels (dilute FeCu alloys).[12–14] Unfortunately, since it is rather difficult to probe the electronic structure of a nanosize embedded particle by using usual experimental methods, the bcc Cu precipitates attract little attention in the field of general electronic structure studies.

Very recently, we applied the positron annihilation technique to the study of bcc Cu precipitates and explored many interesting features of the electronic structure of this metastable Cu phase.[15–17] The positron annihilation technique is a powerful tool because of the fact that positrons in solid annihilate with surrounding electrons into γ photons, which convey important information about the electronic structure around the annihilation site.[18] Especially, our experiments[15–17] show that the positron is a site-selective probe for the nanosize embedded particles in materials. In our first experiment,[15] we measured the coincidence Doppler broadening (CDB) spectra of positron annihilation radiation [the one-dimensional (1D) projection of momentum-density distribution of positron-electron pair along a chosen axis up to high momentum] for polycrystalline FeCu alloys after thermal aging. We found that the CDB spectrum of an Fe 1.0 wt % Cu alloy thermally aged at 550 °C for 2 h is nearly identical with that of fcc Cu bulk. This convinces us that in the sample the positrons are in a quantum-dot-like state, in which the positron wave function is completely confined spatially within the bcc Cu precipitates even free from vacancy-type defects, so that the electronic structure of bcc Cu is exclusively detected. Later, we succeeded in preparing single crystalline bcc Cu precipitates and again, using the quantum-dot-like positron state, we measured the two-dimensional (2D) projection of momentum-density distribution of positron-electron pair at the low-momentum region for bcc Cu by the positron 2D angular correlation of annihilation radiation (2D-ACAR) technique. We observed different 2D-ACAR anisotropy patterns for bcc and fcc Cu. By comparing the experiments and first-principles calculations, we demonstrated that the patterns reflect the characteristic Fermi-surface topologies of these two copper phases.[17]

In this paper, we present systematic first-principles calculations of electronic structures and positron annihilation

characteristics in bcc Cu, fcc Cu, and bcc Fe. The calculations employ the linearized-augmented-plane-wave (LAPW) basis set,[19] so that semicore and core electrons, as well as valence electrons, are accurately described. The calculation based on the generalized gradient approximation (GGA) within the density-functional theory (DFT) well reproduces bulk properties, which confirms the validity of the GGA. We then perform a two-component density-functional calculation on the CDB and obtain good agreement between theory and experiment. As a result, we clarify physical origins of experimentally observed features of the CDB spectra and provide a solid interpretation on experimental results.

II. METHOD

As mentioned in the preceding section, the present work highlights the electronic structures probed by the positron CDB technique. In the CDB experiments, a couple of solid detectors are employed to register, in coincidence, the Doppler shifts in the energies of two annihilation γ photons arising from the longitudinal momentum component of the positron-electron pair. The coincidence measurement much reduces the high background suffered in the usual one-detector DB technique so that the momentum-density distribution (projected to the γ photon emission direction) of the positron annihilations with both the valence and core electrons can be profiled up to a higher-momentum range.[20–23] To calculate the CDB spectrum, it is necessary to describe accurately the valence electrons as well as the core electrons over the whole system. To achieve this, we employ the full-potential LAPW (FLAPW) band-structure method based on the density-functional theory[24,25] in the present work.

We expand the wave functions of the valence electrons and of the semicore electrons (i.e., those high lying and relatively extended core electrons in atoms[26]) by the LAPW basis set.[27,28] For those low-lying core states, the atomic wave functions are employed, which are calculated self-consistently using the scalar-relativistic version of the Schrödinger equation having the spherically averaged crystal potential. The exchange and correlation energy functional of the electrons is calculated within the local-density approximation (LDA),[29] as well as the GGA according to Perdew and co-workers.[30] The Brillouin-zone integration in the self-consistent calculation of charge density is performed using the special *k*-points scheme initiated by Chadi and Cohen.[31,32]

Unlike the electron wave functions, the positron wave function has neither multiple nodes nor rapid oscillation around the core region so that it can be expanded by the pure plane waves uniformly over the system. The positron-electron correlation is calculated based on the two-component density-functional theory (TCDFT).[33] Within this TCDFT, there have been several schemes proposed to handle approximately the correlation effect[33–37] and in this work we chose the well-established LDA of Puska, Seitsonen, and Nieminen.[35] In this scheme, the correlation energy and the enhancement factor are deduced from numerical results for a single positron in homogeneous electron gas: The energy and enhancement factor are calculated by Arponen and Pajanne[38] and by Lantto,[39] respectively. This scheme has been shown by recent applications to be very reliable.[19,40–44]

After determination of the wave functions of the electrons and positron, the 3D momentum-density distributions of the positron-electron pairs, $\rho(\mathbf{p})$, are calculated. The calculational method was described in detail in our previous paper.[19] The experimental CDB spectrum $N(p_z)$ and positron annihilation rate λ (the positron lifetime τ is the inverse of the annihilation rate) are obtained as

$$N(p_z) = \text{const} \times \int \rho(\mathbf{p}) dp_x dp_y , \tag{1}$$

and

$$\lambda = \frac{\pi r_0^2 c}{8\pi^3} \int \rho(\mathbf{p}) dp_x dp_y dp_z . \tag{2}$$

III. RESULTS AND DISCUSSION

A. Cohesive properties

Since there have been many controversies about the structural and cohesive properties of bcc Cu in the previous theoretical studies,[1–6] we here start our calculations from reexamining the equilibrium state of this metastable Cu phase. To estimate the accuracy of the calculations, the cohesive properties of fcc Cu and bcc Fe are also calculated and are compared with the experiments.

We calculate the total energies of the above three systems as functions of atomic volume. In the calculations, the $3d4s$ ($3s3p$) electrons of Cu and Fe atoms are treated as the valence (semicore) electrons. The radii of the muffin-tin (MT) spheres, R_{MT}, are chosen as follows: When the Cu-Cu or Fe-Fe bond length is shorter than 4.26 a.u. (2.25 Å), a contact-type MT sphere is employed; otherwise, R_{MT} is fixed at 2.13 a.u. (1.13 Å). The wave-vector cutoff of the LAPW basis size, K_{cut}, is scaled so that $R_{MT}K_{cut}=12.6$. The spherical harmonic expansions of charge density and potential inside the MT sphere are performed up to $l_{\max}=8$. As for the Brillouin-zone integration, a Monkhorst-Pack-type[32] *k*-mesh containing $25\times25\times25$ ($21\times21\times21$) *k* points is sampled for bcc Cu and bcc Fe (fcc Cu). These convergence parameters are chosen after a careful test; as a result, the error of the calculated energies is estimated to be less than 1.0 meV.

Figure 1 presents the total energies calculated within the GGA, where the total energy of a free Cu (Fe) atom is taken to be the energy zero for bcc Cu and fcc Cu (bcc Fe). The equations of state, namely, the pressures as functions of atomic volume, are calculated as the volume derivations of the total energies, and the one of bcc Cu is shown in the inset of Fig. 1. The resulting cohesive energies, lattice parameters, and bulk moduli, together with those values calculated within the LDA, are listed in Table I in comparison with the available experimental results. In both the calculations using the LDA and GGA (Fig. 1), we observe only a single metastable state in bcc Cu, in good agreement with the recent calculations.[3–6] Moreover, as shown in Table I, the GGA gives a better reproduction of the experimental results. For

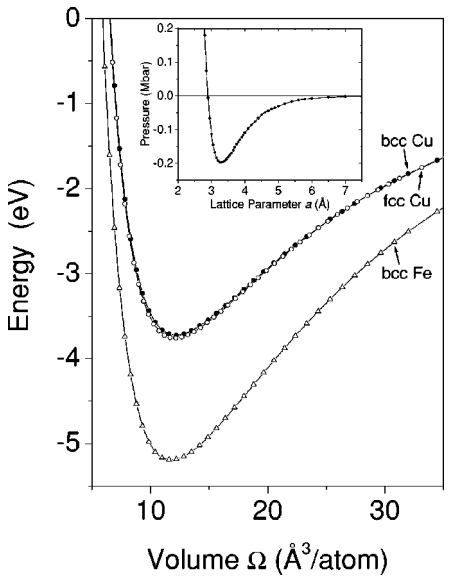

FIG. 1. Calculated total energy as a function of atomic volume for bcc Cu (solid circles), fcc Cu (open circles), and bcc Fe (open triangles). The inset shows the equation of state of bcc Cu, where to see clearly the equilibrium lattice parameter the pressure is presented as a function of lattice parameter instead of the atomic volume.

fcc Cu and bcc Fe, the maximum deviations between the GGA calculations and the experiments are about 0.3% (lattice parameters), 21.3% (cohesive energies), and 30.7% (bulk moduli); while those deviations between the LDA calculations and the experiments are 3.8%, 47.9%, and 38.0%, respectively. Since the GGA is more reliable than the LDA, we adopt the GGA electron wave functions in our positron calculations hereafter.

TABLE I. Calculated ground-state properties [equilibrium lattice parameters (a), cohesive energies (E_{coh}), and bulk moduli (B)] of ferromagnetic iron (bcc Fe), fcc copper (fcc Cu), and bcc copper (bcc Cu) in comparison with available experiments. The calculations use the full-potential linearized-augmented-plane-wave method. The electron exchange and correlation potentials are constructed within the local-density approximation (LDA) according to Cerpley and Alder (Ref. 29), and within the generalized gradient approximation (GGA) according to Perdew and co-workers (Ref. 30). The calculations for bcc Fe are spin polarized.

		a (Å)	E_{coh} (eV)	B (Mbar)
bcc Fe	LDA	2.76	6.33	2.07
	GGA	2.86	5.19	1.71
	Expt. [a]	2.87	4.28	1.68
fcc Cu	LDA	3.58	4.21	1.89
	GGA	3.62	3.76	1.79
	Expt. [a]	3.61	3.49	1.37
bcc Cu	LDA	2.84	4.14	1.88
	GGA	2.90	3.72	1.41
	Expt.	2.87 [b], 2.89 [c]		

[a]Reference 45.
[b]Epitaxial bcc Cu films on Fe(001) substrates, Ref. 7.
[c]Epitaxial bcc Cu films on Ag(001) substrates, Ref. 9.

The present calculations show that the equilibrium lattice parameter of bcc Cu is 2.90 Å (Fig. 1 and Table I). This value agrees reasonably well with those of recent theoretical studies (for instance, 2.86 Å by Lu, Wei, and Zunger[4] using the FLAPW method within LDA and 2.90 Å by Zhou, Lai, and Wang[5] using the linear muffin-tin orbital method within the GGA). Our value is also close to the experimental one observed in the epitaxial Cu films [2.87 Å on Fe(001), (Ref. 7) or 2.89 Å on Ag(001),[9] it should be noticed that these experimental values were actually estimated as the surface lattice parameters of the substrates].

The cohesive energy of metastable bcc Cu is close to that of stable fcc Cu, suggesting that this metastable phase is likely to appear under some condition, e.g., Cu precipitated in Fe matrix. The difference between the calculated equilibrium lattice parameters of bcc Cu and bcc Fe is rather small (0.04 Å), indicating that the bcc Cu precipitates in Fe matrix only suffer from very small strains, so that a nearly perfect coherence between the lattices of the precipitates and matrix is possible for their smaller sizes.

B. Coincidence Doppler broadening of positron annihilation radiation

Using the above equilibrium-state structures, we calculate in this section the momentum-density distributions of the positron-electron pairs in bcc Cu, fcc Cu, and bcc Fe. In our calculations, we employ the electron wave functions at the equilibrium states calculated within the GGA using the same parameters as presented in the preceding section. The positron wave function at the Γ point is expanded by the plane-wave basis set, whose cut-off wave vector is carefully chosen after test [13.6 a.u. (25.7 $Å^{-1}$)]. The 3D momentum-density distributions of the positron-electron pairs are calculated in the region up to $80\times10^{-3}m_0c$ ($1m_0c = 137.036$ a.u.).

Figure 2 presents the calculated CDB spectra for these three systems projected in the crystallographic direction [100]. In the figure, we decompose each spectrum into three components, which correspond to positron annihilation with the valence electrons, semicore electrons, and core electrons. It is found that the CDB spectra for bcc Cu and fcc Cu are very similar. In both cases, we observe a rapid drop in momentum density around $5\times10^{-3}m_0c$. This rapid drop is followed by a broad, hill-like momentum-density distribution extended up to about $30\times10^{-3}m_0c$. As shown by the partial CDB contributions in Fig. 2, these features are due to the positron-valence-electron annihilation, which dominates the shape of the total spectrum in the above momentum region (this region is somewhat wide compared with those in Al, graphite,[19] and Si). With further increase in the momentum, the valence-electron contribution becomes invisible; instead, the positron annihilations with the semicore and core electrons become the dominant components.

The above-mentioned momentum-density drops lie near the Fermi momenta. As shown in Fig. 3, the highest occupied

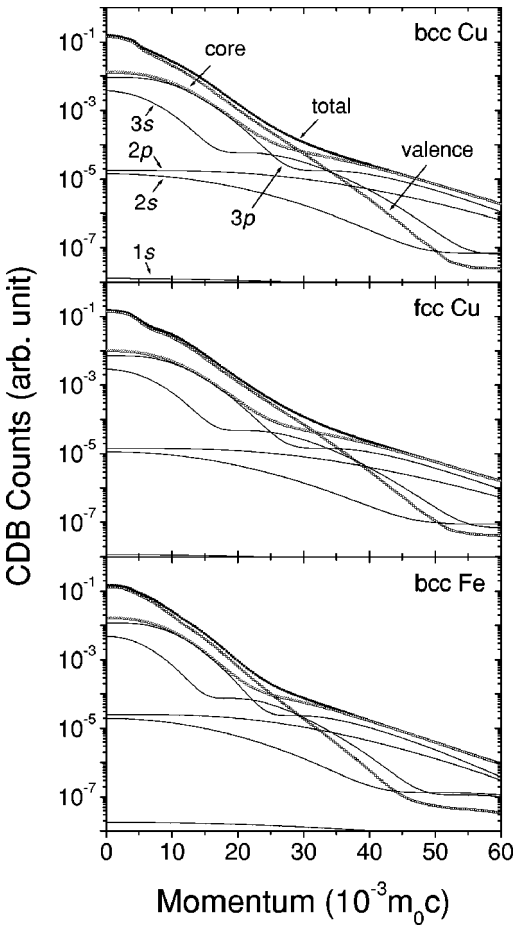

FIG. 2. Calculated coincidence Doppler broadening spectra along the [100] direction for bcc Cu (upper), fcc Cu (middle), and bcc Fe (lower). For each spectrum, partial contributions of positron annihilations with valence and core electrons (which are further decomposed into the contributions of $1s$, $2s$, $2p$, $3s$, and $3p$ electrons) are also presented.

valence band in bcc Cu crosses the Fermi-energy level nearly isotropic in any direction starting from the Γ point, except for those around the [110] axis (as well as its equivalent axes). Thus, in the first Brillouin zone, bcc Cu has a nearly spherical Fermi surface with 12 necks connected to the (110) and other (11) equivalent zone boundaries. Similar to bcc Cu, fcc Cu also has a nearly isotropic Fermi surface with eight necks along the [111] and equivalent directions.[45](The highest occupied valence band in fcc Cu is below the Fermi level along these directions [Fig. 3(b)].) Due to this nearly-free-electron character of the electronic structure, the Fermi momenta of bcc Cu and fcc Cu depend mainly on their equilibrium atomic volumes. As shown in Fig. 1, the equilibrium atomic volumes of bcc Cu and fcc Cu are very similar, so that the calculated Fermi momenta for both Cu systems are close, for instance, $5.18\times10^{-3}m_0c$ for bcc Cu and $5.67\times10^{-3}m_0c$ for fcc Cu in the [100] direction. These values are only slightly different from those estimated from the nearly-free-electron model ($5.19\times10^{-3}m_0c$ and $5.23\times10^{-3}m_0c$ for bcc Cu and fcc Cu, respectively).

In addition to the half-filled highest band, there are other five fully occupied valence bands in bcc Cu originating from

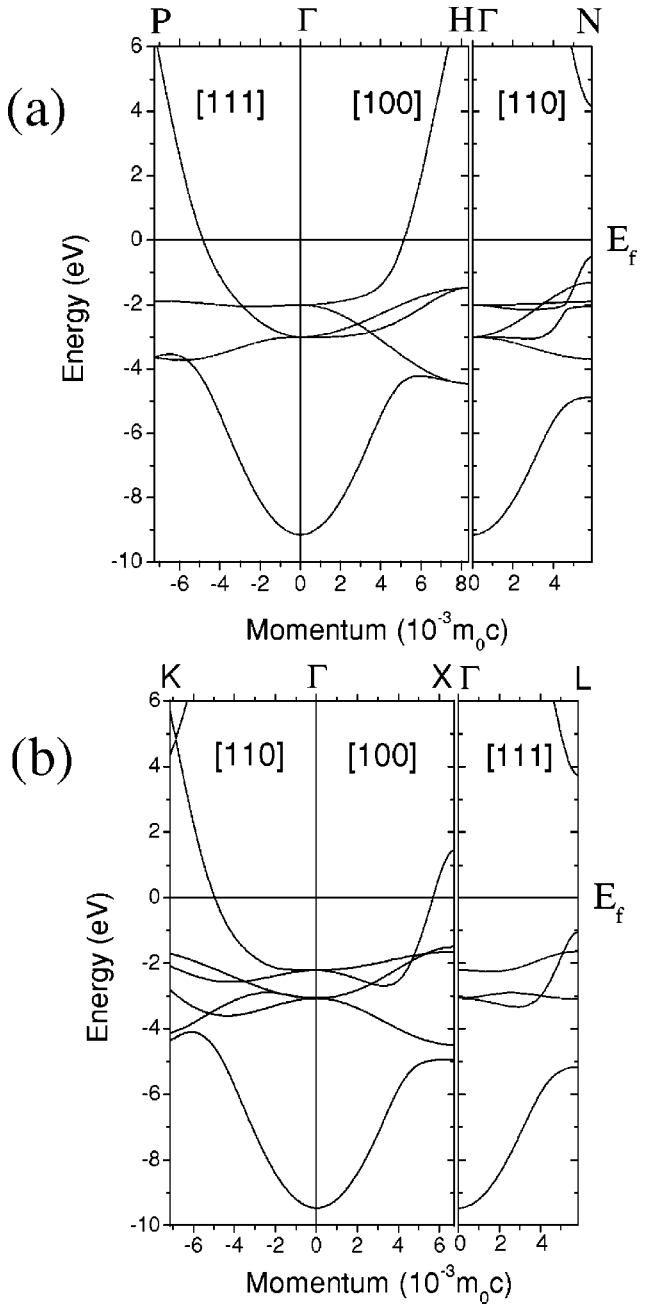

FIG. 3. Calculated band structure for (a) bcc Cu and (b) fcc Cu at the equilibrium lattice constant along [100], [110], and [111] directions. Energies are in eV measured relative to the Fermi energy level.

the closed $3d^{10}$ shell of the Cu atom (Fig. 3). These bands contribute to a d-like momentum-density distribution (namely the broad, hill-like background in Fig. 2) dominating the shape of the total CDB spectrum up to $30\times10^{-3}m_0c$. Especially, due to the weak interatomic interaction of the closed $3d^{10}$ shells of the Cu atoms (as evidenced by the smaller cohesive energies in bcc Cu and fcc Cu than that in bcc Fe), the crystal environment modifies little this atomic-orbital-like $3d$ electron momentum-density distribution, so that the CDB spectra in both bcc Cu and fcc Cu are similar up to the highest momentum. Moveover, since the

TABLE II. Calculated positron-valence-electron (λ_v) and positron-core-electron (λ_c) annihilation rates in bcc Cu, fcc Cu, and bcc Fe. Here λ_c is a summation of positron annihilations with both semicore and core electrons. Relative weights of λ_c and λ_v in total annihilation rate ($\lambda_c+\lambda_v$) are listed in parentheses. The calculated positron lifetimes (as the inverses of the total annihilation rates) are compared with the experiments.

	λ_c (ns^{-1})	λ_v (ns^{-1})	τ_{cal} (ps)	τ_{exp} (ps)
bcc Cu	1.27 (13.5%)	8.13 (86.5%)	106	108[a]
fcc Cu	1.00 (10.6%)	8.34 (89.4%)	107	110
bcc Fe	1.50 (15.6%)	8.13 (84.4%)	104	106

[a]Measured by using an Fe 1.0 wt % Cu alloy thermally aged at 550 °C for 2 h.

momentum densities below and above the Fermi momentum in these two Cu systems are dominated, respectively, by the positron annihilations with the nearly free *s* electrons and more localized *d* electrons, a decrease in the positron-electron enhancement effect is expected when the momentum increases across the Fermi momentum. This fact further highlights the momentum-density drops around $5\times10^{-3}m_0c$ for both Cu systems.

As for bcc Fe, the Fermi surface mainly originates from the partially filled *d* bands, thus, there is no significant change in the positron-electron enhancement effect when the momentum increases across the Fermi momentum. Especially, since the topology of the Fermi surface of bcc Fe is very complicated, no clear Fermi-surface break can be expected in the 1D projection of the momentum-density distribution. Indeed, the CDB spectrum in bcc Fe is continuous over the whole calculated momentum region (Fig. 2). Moreover, since the Fe atom has an open $3d$ shell with only six *d* electrons, the *d*-like momentum-density distribution in bcc Fe becomes invisible from $25\times10^{-3}m_0c$, a relatively lower momentum compared with those in bcc Cu and fcc Cu.

C. Comparison with experiments

In this section, we compare the theoretical results with the experimental ones to clarify the physical origin of recent experimental observations. In Table II, we present the calculated positron lifetimes together with the experimental results. In Fig. 4, the calculated CDB spectra projected in [100] direction are convoluted with the experimental resolution (1.1 keV, about $4.3\times10^{-3}m_0c$) and are compared with the experiments. In this figure, the CDB spectra of fcc Cu and bcc Fe were measured by using single crystals with the projection direction of [100] (details about the experiments can be found in our previous paper[15]), while the spectrum of bcc Cu was measured using a polycrystalline Fe 1.0 wt % Cu alloy after thermal aging at 550 °C for 2 h (further prolonging the aging time to 10 h leads to no change in the CDB spectrum). As discussed in our previous work,[15] we believe that in this alloy sample the positrons are completely confined within the bcc Cu precipitates, so that the momentum-density distribution of bcc Cu is exclusively detected. Because of the polycrystalline used in the experiment, this spectrum corresponds to the orientation-averaged projection of the momentum-density distribution in bcc Cu. However, this averaging effect is rather trivial for the discussion presented later, since the momentum-density distribution in bcc Cu is nearly isotropic at the high-momentum region due to the atomic-wave-function-like character of the closed $3d$ shell.

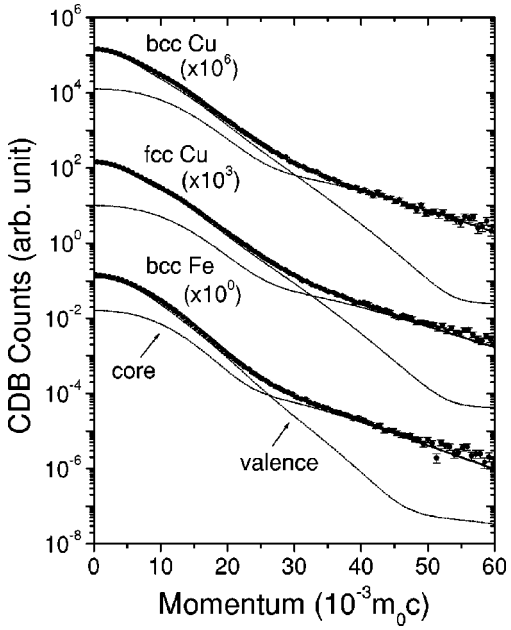

FIG. 4. Comparison between calculated (thick lines) and experimental (solid circles with error bars) coincidence Doppler broadening spectra for bcc Cu (upper), fcc Cu (middle), and bcc Fe (lower). All the calculations are projected along [100] direction and are convoluted with the experimental resolution of 1.1 keV $\sim4.3\times10^{-3}m_0c$. Dashed lines denote partial contributions of positron annihilations with valence and core electrons. The experiments were measured along [100] for fcc Cu and bcc Fe; while that for bcc Cu was measured by using a polycrystalline Fe 1.0 wt. % Cu alloy thermally aged at 550 °C for 2 h so that only an angle-averaged projection was obtained. The spectra are normalized and are shifted vertically as labeled in the figure for comparison.

As shown in Table II and Fig. 4, the calculations are in good agreement with the experiments for all the systems (the calculated positron lifetimes also agree well with other reported calculations[41]). In particular, the calculated CDB spectra are found to well reproduce the experiments over the entire measurable momentum range, indicating that the present all-electron and full-potential method is very suitable for the positron CDB studies for the transitional metals. It is also noticed that, because of the smearing effect of the resolution inherent in the CDB spectrum using two Ge detectors, the characteristic features of momentum-density distribution discussed in the preceding section becomes less emphasized. Following the method employed in our previous experimental studies[15,16] (which is initiated by Lynn *et al.*[20–22]), we extract the CDB ratio spectra for bcc Cu and fcc Cu, by taking the spectrum of bcc Fe as a reference (Fig. 5). In Fig. 5, the calculated ratios are further decomposed into the contributions of the valence-electron and core-electron annihila-

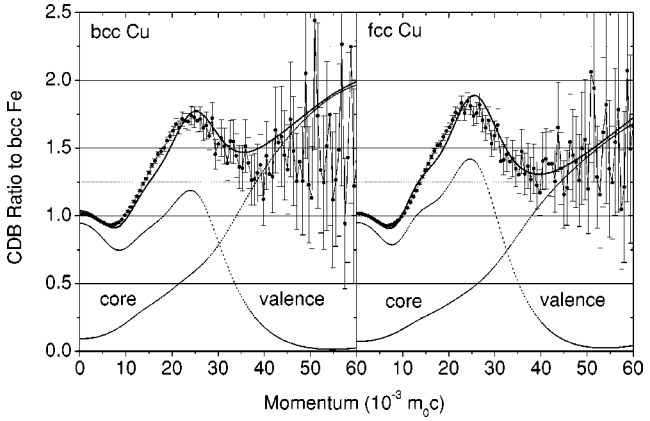

FIG. 5. Calculated (thick lines) and experimental (solid circles with error bars) ratio spectra of coincidence Doppler broadening along [100] direction for bcc Cu (left) and fcc Cu (right) with respect to that of bcc Fe. The calculated ratios are further decomposed into the partial contributions of positron annihilations with valence and core electrons. For comparison, all the calculational spectra (including the partial contributions) are convoluted with the experimental resolution before extracting ratios. The experimental ratio spectra were extracted using the experimental results presented in Fig. 4.

tions. As shown in this figure, the agreement between experiment and theory is satisfactory. We clearly observe in both the experiments and calculations a ratio valley around $7\times10^{-3}m_0c$ and a pronounced ratio peak around $25\times10^{-3}m_0c$. These signals have been considered to be the fingerprints specific to the Cu atoms and are important in interpreting recent experimental results.[15,16]

It is now clear that the above signals originate from the positron annihilations with the valence electrons of the Cu atoms (as shown by the partial ratio contributions in Fig. 5). Since there is a rapid drop in momentum density around $5\times10^{-3}m_0c$ (Fermi momenta) in bcc Cu and fcc Cu, while the momentum-density distribution is smooth around this region in bcc Fe; we observe a characteristic ratio valley around $7\times10^{-3}m_0c$ due to the Fermi-surface break and the decrease of the positron-electron enhancement effect across the Fermi surface as discussed in above (the valley position is slightly shifted due to the resolution). Moreover, since the Cu atoms have more $3d$ valence electrons ($3d^{10}$ of Cu versus $3d^6$ of Fe), the ratios of the CDB spectra of both Cu systems relative to that of bcc Fe increase continuously with increasing the momentum from the Fermi momentum up to $25\times10^{-3}m_0c$ (Fig. 5). By further increasing the momentum from this point, however, the reference spectrum (the CDB spectrum of bcc Fe) changes its dominant component from that of the $3d$ valence electrons to that of the semicore and core electrons, so that the maximum ratio peaks appear around $25\times10^{-3}m_0c$.

Finally, we discuss the subtle difference between the CDB spectra in bcc Cu and fcc Cu. As explored clearly by the ratio spectra in Fig. 5, the CDB spectrum in bcc Cu is slightly different from that in fcc Cu. The momentum density of the positron annihilation with the valence electrons (the semi-

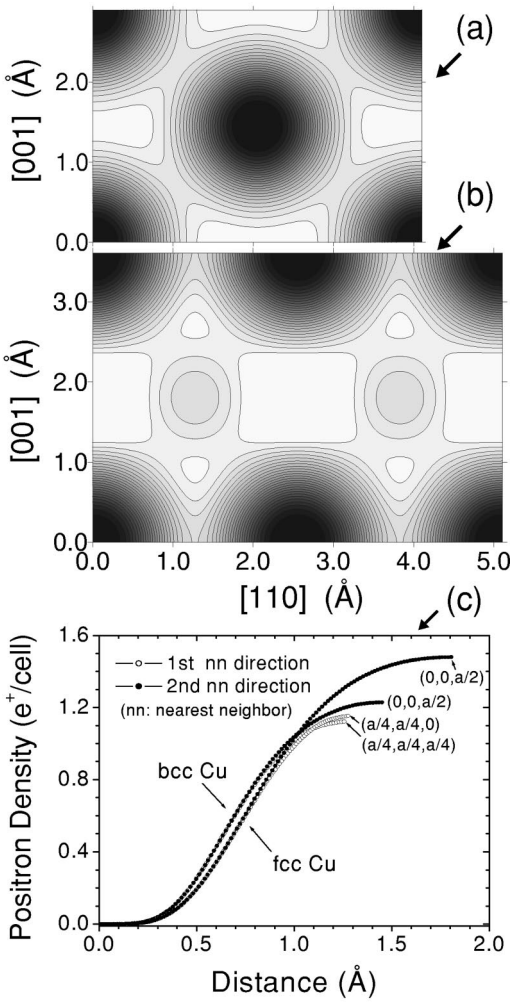

FIG. 6. Calculated positron density distribution on $[1\bar{1}0]$ plane for (a) bcc Cu and (b) fcc Cu, where white (black) denotes high (low) positron density. In (c) the positron densities along the first nearest-neighbor Cu-Cu binding direction ([111] for bcc Cu and [110] for fcc Cu) and along the second nearest-neighbor Cu-Cu binding direction ([001] for both) in these systems are compared (the positron densities are normalized in the primitive cells).

core and core electrons) in bcc Cu is definitely smaller (larger) than that in fcc Cu. As a result, the amplitude of the characteristic ratio peak around $25\times10^{-3}m_0c$ in bcc Cu is reduced slightly (by 5.8% in experiment or 6.2% in theory) from that in fcc Cu, because in this momentum region the positron-valence-electron annihilations dominate the shapes of the CDB ratio curves. Furthermore, with increasing the momentum beyond about $30\times10^{-3}m_0c$, the CDB ratio in bcc Cu becomes larger than that in fcc Cu since in this high-momentum region the positron annihilations with the semicore and core electrons dominate the CDB ratio shapes. These differences are also represented explicitly by the partial annihilation rates listed in Table II.

The variation of the positron annihilations with the semicore and core electrons in these two Cu systems provides an important clue to understand the above results. The signifi-

cant change in the annihilation characteristics of these tightlybound electrons (Fig. 5 and Table II) actually excludes the possibility that the electron wave functions are the dominant reason for the observations, because there is no considerable difference in the semicore and core electronic structures for both systems. Thus, we expect that the positron wave functions play a more essential role. To verify this, we present the calculated positron density distributions on the $[1\bar{1}0]$ plane for bcc Cu and fcc Cu in Figs. 6(a) and 6(b), respectively. Furthermore, the positron densities along the first- and second-nearest-neighbor Cu-Cu bonds in these two systems are compared in Fig. 6(c). From Fig. 6, it is clearly observed that the positron density around the nucleus (around bond centers) in bcc Cu is higher (lower) than that in fcc Cu. As a result, the positron has a larger (smaller) possibility to sample the semicore and core (valence) electrons in bcc Cu than in fcc Cu (namely, the positron annihilation in the former is of a more localized character). Therefore, in bcc Cu there is the slightly reduced ratio peak in the valence-electron-dominated momentum region $(25\times10^{-3}m_0c)$ accompanied by the larger ratios in the (semicore and core)-electron-dominated momentum region $(>30\times10^{-3}m_0c)$. This definite difference is important since it enables an accurate estimation of the positron annihilation proportion in the bcc Cu precipitates in the case where the complete confinement of the positrons into the precipitates is absent so that both the Fe matrix and the precipitates of the FeCu alloy are sampled by the positrons.

It should be noticed that, in the experiments, the positrons are localized and annihilate in the bcc Cu precipitates of about 1 nm (at most less than 2 nm) embedded in Fe matrix,[15] while the size effects of the embedded particles upon the positronic and electronic structures are ignored in the present calculations. To clarify these interesting effects, further calculations for the systems consisting of the precipitates and the host matrix are necessary but are beyond the scope of this study.

IV. CONCLUSION

Using the all-electron full-potential method and density-functional theory, we performed electronic structure calculation on bcc Cu, fcc Cu, and bcc Fe. Furthermore, we calculated the positron-electron pair momenta using the two-component density-functional theory. The GGA within the density-functional theory was found to well reproduce bulk properties. Based on the calculated results, we concluded that the metastable bcc and stable fcc phases of copper have very similar cohesive energies and the lattice constants of bcc Cu and bcc Fe are very close, which indicates that the bcc Cu precipitates in Fe matrix have very small strain energies. These results support the experimental suggestion that the atomic positions of the bcc Cu precipitates in Fe matrix are nearly coherent to those of the matrix.[11,15]

The calculated momentum-density distributions of positron-electron pairs of bcc and fcc coppers are very similar but there is subtle difference around $25\times10^{-3}m_0c$. These momentum-density distributions were found to be quite different from that of bcc Fe; thus, the analysis of the observed CDB spectra is expected to give important information on the Cu precipitates in Fe matrix. Indeed, by comparing the calculated and measured CDB spectra, we confirmed the previous experimental conclusion:[15] In the Fe 1.0 wt % Cu alloy after thermal aging at 550 °C for 2 h, the observed spectra originate from the completely confined positrons in the bcc Cu precipitates.

ACKNOWLEDGMENTS

The authors would like to express their sincere thanks to the Information Science Group of the Institute for Materials Research, Tohoku University, for its continuous support of using the Hitachi SR8000 supercomputing system. This work was partly supported by JAERI's Nuclear Research Promotion Program (JANP) and by Grant-in-Aid for Scientific Research of the Ministry of Education, Culture, Sports, Science and Technology (Grants Nos. 12358005, 12640334, and 13305044).

[1] M.H. Kang, R.C. Tatar, E.J. Mele, and P. Soven, Phys. Rev. B **35**, 5457 (1987).
[2] I.A. Morrison, M.H. Kang, and E.J. Mele, Phys. Rev. B **39**, 1575 (1989).
[3] J.R. Chelikowsky and M.Y. Chou, Phys. Rev. B **38**, 7966 (1988).
[4] Z.W. Lu, S.-H. Wei, and A. Zunger, Phys. Rev. B **41**, 2699 (1990).
[5] Y. Zhou, W. Lai, and J. Wang, Phys. Rev. B **49**, 4463 (1993).
[6] S. Jeong, Phys. Rev. B **53**, 13 973 (1996).
[7] Z.Q. Wang, S.H. Lu, Y.S. Li, F. Jona, and P.M. Marcus, Phys. Rev. B **35**, 9322 (1987).
[8] B. Heinrich, Z. Celinski, J.F. Cochran, W.B. Muir, J. Rudd, Q.M. Zhong, A.S. Arrott, K. Myrtle, and J. Kirschner, Phys. Rev. Lett. **64**, 673 (1990).
[9] H. Li, D. Tian, J. Quinn, Y.S. Li, F. Jona, and P.M. Marcus, Phys. Rev. B **43**, 6342 (1991).
[10] C. Schmidt, F. Ernst, M.W. Finnis, and V. Vitek, Phys. Rev. Lett. **75**, 2160 (1995).
[11] S.R. Goodman, S.S. Brenner, and J.R. Low, Metall. Trans. **4**, 2363 (1973).
[12] W.J. Phythian and C.A. English, J. Nucl. Mater. **205**, 162 (1993), and references cited therein.
[13] P.J. Othen, M.L. Jenkins, and G.D.W. Smith, Philos. Mag. A **70**, 1 (1994).
[14] G.R. Odette, C.L. Liu, and B.D. Wirth, in *Microstructure Evolution During Irradiation*, edited by I. M. Robertson, G. S. Was, L. W. Hobbs, and T. Diaz de la Rubia, Mater. Res. Soc. Symp. Proc. **439** (Materials Research Society, Pittsuburgh, 1997), p. 457.
[15] Y. Nagai, M. Hasegawa, Z. Tang, A. Hempel, K. Yubuta, T. Shimamura, Y. Kawazoe, A. Kawai, and F. Kano, Phys. Rev. B **61**, 6574 (2000).
[16] Y. Nagai, Z. Tang, M. Hasegawa, T. Kanai, and M. Saneyasu, Phys. Rev. B **63**, 134110 (2001).
[17] Y. Nagai, T. Chiba, Z. Tang, T. Akahane, T. Kanai, M. Hasegawa,

M. Takenaka, and E. Kuramoto, Phys. Rev. Lett. **87**, 176402 (2001).
[18] *Positron Solid-State Physics*, edited by W. Brandt and A. Dupasquier (North-Holland, Amsterdam, 1995).
[19] Z. Tang, M. Hasegawa, Y. Nagai, M. Saito, and Y. Kawazoe, Phys. Rev. B **65**, 045108 (2002).
[20] K.G. Lynn, J.R. MacDonald, R.A. Boie, L.C. Feldman, J.D. Gabbe, M.F. Robbins, E. Bonderup, and J. Golovchenko, Phys. Rev. Lett. **38**, 241 (1977).
[21] K.G. Lynn, J.E. Dickman, W.L. Brown, M.F. Robbins, and E. Bonderup, Phys. Rev. B **20**, 3566 (1979).
[22] P. Asoka-Kumar, M. Alatalo, V.J. Ghosh, A.C. Kruseman, B. Nielsen, and K.G. Lynn, Phys. Rev. Lett. **77**, 2097 (1996).
[23] K. Saarinen, J. Nissilä, H. Kauppinen, M. Hakala, M.J. Puska, P. Hautojärvi, and C. Corbel, Phys. Rev. Lett. **82**, 1883 (1999).
[24] H.J.F. Jansen and A.J. Freeman, Phys. Rev. B **30**, 561 (1984).
[25] L.F. Mattheiss and D.R. Hamann, Phys. Rev. B **33**, 823 (1986).
[26] D.J. Singh, *Planewaves, Pseudopotentials and the LAPW Method*, (Kluwer Academic, Boston, 1994).
[27] O.K. Anderson, Phys. Rev. B **12**, 3060 (1975).
[28] D.D. Koelling and G.O. Arbman, J. Phys. F: Met. Phys. **5**, 2041 (1975).
[29] D.M. Ceperley and B.J. Alder, Phys. Rev. Lett. **45**, 566 (1980); J.P. Perdew and A. Zunger, Phys. Rev. B **23**, 5048 (1981).
[30] J.P. Perdew and Y. Wang, Phys. Rev. B **45**, 13 244 (1992); J.P. Perdew, J.A. Chevary, S.H. Vosko, K.A. Jackson, M.R. Pederson, D.J. Singh, and C. Fiolhais, *ibid.* **46**, 6671 (1992).
[31] D.J. Chadi and M.L. Cohen, Phys. Rev. B **8**, 5747 (1973).
[32] H.J. Monkhorst and J.D. Pack, Phys. Rev. B **13**, 5188 (1976).
[33] E. Boroński and R.M. Nieminen, Phys. Rev. B **34**, 3820 (1986).
[34] M.J. Puska and R.M. Nieminen, Rev. Mod. Phys. **66**, 841 (1994).
[35] M.J. Puska, A.P. Seitsonen, and R.M. Nieminen, Phys. Rev. B **52**, 10 947 (1995).
[36] B. Barbiellini, M.J. Puska, T. Korhonen, A. Harju, T. Torsti, and R.M. Nieminen, Phys. Rev. B **53**, 16 201 (1996).
[37] A. Rubaszek, Z. Szotek, and W.M. Temmerman, Phys. Rev. B **58**, 11 285 (1998).
[38] J. Arponen and E. Pajanne, Ann. Phys. (N.Y.) **121**, 343 (1979).
[39] L.J. Lantto, Phys. Rev. B **36**, 5160 (1987).
[40] M. Alatalo, B. Barbiellini, M. Hakala, H. Kauppinen, T. Korhonen, M.J. Puska, K. Saarinen, P. Hautojärvi, and R.M. Nieminen, Phys. Rev. B **54**, 2397 (1996).
[41] T. Korhonen, M.J. Puska, and R.M. Nieminen, Phys. Rev. B **54**, 15 016 (1996).
[42] P.E. Mijnarends, A.C. Kruseman, A. van Veen, H. Schut, and A. Bansil, J. Phys.: Condens. Matter **10**, 10 383 (1998).
[43] Z. Tang, M. Hasegawa, T. Chiba, M. Saito, H. Sumiya, Y. Kawazoe, and S. Yamaguchi, Phys. Rev. B **57**, 12 219 (1998).
[44] V.J. Ghosh, M. Alatalo, P. Asoka-Kumar, B. Nielsen, K.G. Lynn, A.C. Kruseman, and P.E. Mijnarends, Phys. Rev. B **61**, 10 092 (2000).
[45] See, for example, C. Kittel, *Introduction to Solid State Physics*, 7th ed. (Wiley, New York, 1996).